Improving Sensitivity in Ultrasound Molecular Imaging by Tailoring Contrast Agent Size Distribution: In Vivo Studies

Jason E. Streeter, **Ryan Gessner**, **Iman Miles**, and **Paul A. Dayton**
Joint Department of Biomedical Engineering, University of North Carolina–North Carolina State University, Chapel Hill, NC.

Abstract

Molecular imaging with ultrasound relies on microbubble contrast agents (MCAs) selectively adhering to a ligand-specific target. Prior studies have shown that only small quantities of microbubbles are retained at their target sites, therefore, enhancing contrast sensitivity to low concentrations of microbubbles is essential to improve molecular imaging techniques. In order to assess the effect of MCA diameter on imaging sensitivity, perfusion and molecular imaging studies were performed with microbubbles of varying size distributions. To assess signal improvement and MCA circulation time as a function of size and concentration, blood perfusion was imaged in rat kidneys using nontargeted size-sorted MCAs with a Siemens Sequoia ultrasound system (Siemans, Mountain View, CA) in cadence pulse sequencing (CPS) mode. Molecular imaging sensitivity improvements were studied with size-sorted $\alpha_v\beta_3$-targeted bubbles in both fibrosarcoma and R3230 rat tumor models. In perfusion imaging studies, video intensity and contrast persistence was ≈8 times and ≈3 times greater respectively, for "sorted 3-micron" MCAs (diameter, 3.3 ± 1.95 μm) when compared to "unsorted" MCAs (diameter, 0.9 ± 0.45 μm) at low concentrations. In targeted experiments, application of sorted 3-micron MCAs resulted in a ≈20 times video intensity increase over unsorted populations. Tailoring size-distributions results in substantial imaging sensitivity improvement over unsorted populations, which is essential in maximizing sensitivity to small numbers of MCAs for molecular imaging.

MICROBUBBLE CONTRAST AGENTS (MCAs) are used to improve ultrasound imaging studies by increasing sensitivity between blood and surrounding tissue.[1–3] In clinical practice, MCAs are used as blood-pool agents in applications that monitor blood flow, such as myocardial perfusion.[1,2,4] However, developments in molecular imaging provide a range of new targeting applications for contrast-enhanced ultrasonography, including, but not limited to, the diagnosis of myocarditis, evaluation of myocardial infarction, assessment of transplant rejection, ischemic memory imaging, and early-stage detection and treatment of solid tumors.[4,5] Targeted MCAs are acoustically active bubbles fitted with a high-affinity targeting ligand. Once bound to their targets, these MCAs enhance the acoustic signal from pathologic tissue that might otherwise be difficult to distinguish from normal tissues.[1,2,4] Integrin or other ligand expression on the diseased tissue allows the targeted MCAs to adhere to the endothelial surface, thus facilitating detection with ultrasound. In recent years, targeted agents have been successfully used for noninvasive imaging of tumor angiogenesis and dysfunctional endothelium, but backscatter intensity is relatively weak owing to the small populations retained during targeting.[2,6–10] This poor binding efficiency necessitates

signal amplification in targeted imaging applications, thus providing the motivation to maximize the sensitivity to bound MCAs.[2,4,11]

Owing to the small percentage of bound MCAs at their target sites, research in targeted ultrasound imaging has focused mainly on improvement of the contrast sensitivity through improved ligands and adhesion schemes, detection methods, and contrast delivery mechanisms.[1,2, 6,11−17] However, over the last several years, more attempts have been made to improve contrast sensitivity by optimizing the echogenicity of the contrast agents themselves. Talu and colleagues proposed that increasing the monodispersity of a microbubble population may improve imaging sensitivity.[6] Theory predicts an increase in ultrasound backscatter intensity as a function of microbubble cross-sectional area and therefore size:

$$I = \frac{\mathbf{I}_o \sigma}{4\pi z^2},$$

(1)

where I_o is incident intensity, σ is the microbubble scattering cross-sectional area, and z is the distance between the transducer and the scattering microbubble.[18] In an in vitro study of the acoustic response of monodisperse contrast agents, Kaya and colleagues determined that signal amplitude could be increased both by matching the imaging frequency to the bubbles' resonant frequency and by increasing the diameter of the microbubbles.[19] Sirsi and colleagues recently demonstrated improvements in contrast to tissue ratio in the mouse kidney with high-frequency contrast imaging as a function of microbubble diameter.[20] Because of the significance of microbubble size in the acoustic response, recent interest has involved new production and sorting methods for MCAs, including centrifugation techniques, microfluidics, and electrohydrodynamic atomization.[21−26] In addition to echogenicity, the bloodstream persistence of a microbubble is directly correlated to the initial radius of an MCA by the dissolution behavior governing lipid-shelled microbubbles, and bubble accumulation in targeted tissues is affected by circulation persistence.[27,28] It should be noted, however, that bloodstream persistence is a complex physiologic phenomenon that depends on several other environmental factors that are not discussed in this article.[28]

The contrast agent currently approved by the Food and Drug Administration (FDA), Definity (Lantheus Medical Imaging, Billerica, MA), has a polydisperse distribution with the mean diameter of around 1 μm (diameter 1.0 ± 0.83 μm, as tested in this study) and a concentration of $\approx 1 \times 10^{10}$ #/mL.[29] This distribution is characteristic of many types of lipid-shelled microbubbles, which are formed by sonic or mechanical agitation, two common formulation techniques for targeted and nontargeted MCAs.[6] For standard perfusion imaging, MCA size distribution has not been a limitation because typically billions of microbubbles are administered intravascularly, providing plenty of image contrast. However, for targeted imaging applications, relatively small populations of adherent MCAs provide weak backscatter intensity and limit imaging sensitivity.[2,6,9]

In this article, we demonstrate in vivo that the improvement of contrast sensitivity in molecular imaging and perfusion imaging applications can be achieved by increasing the mean diameter in MCA populations. We formulated lipid-encapsulated MCAs and obtained distinct size distributions for acoustic testing using centrifugation methods optimized by Feshitan and colleagues.[22] In nontargeted perfusion experiments, size-sorted microbubble distributions and unsorted distributions similar to current FDA-approved lipid-shelled contrast agents were imaged in vivo in the rat kidney using a Sequoia ultrasound system (Siemens, Mountain View, CA). Cadence pulse sequencing (CPS) mode was used in all

studies. CPS is a nondestructive contrast-specific imaging mode developed by Siemens, which has been used for both perfusion and molecular imaging.[30] For perfusion studies, we compare video intensities for administered MCA doses on the order of 150 μL at a concentration of $\approx 6 \times 10^8$ #/mL, similar to concentrations used in previous perfusion studies.[29,31,32] Perfusion imaging studies, at dose concentrations down to 20 times smaller (150 μL at $\approx 3 \times 10^7$ #/mL), were also performed to observe any contrast sensitivity improvement at extremely low concentrations. For molecular imaging of angiogenesis, size-sorted microbubble distributions conjugated with a cyclic Arginine-Glycine-Aspartic acid (RGD) peptide were acoustically evaluated in vivo using two different tumor models to illustrate the contrast sensitivity improvements with these targeted distributions.[10,33]

Materials and Methods

MCA Preparation and Isolation

Various MCA distributions were obtained and characterized for targeted and nontargeted in vivo experiments. The method used to create the characteristic size distributions is based on differences in buoyancy forces for different microbubble sizes and was recently described in detail by Feshitan and colleagues.[22] A centrifugation procedure allows rapid preferential selection of different diameter distributions. For this article, we chose to examine sorted distributions with mean diameters of 1.1 ± 0.43 μm and 3.3 ± 1.95 μm (Figure 1), which were isolated using the centrifugation process. An unsorted polydisperse distribution (diameter 0.9 ± 0.45 μm), similar to the FDA-approved MCA Definity (diameter 1.0 ± 0.83 μm), was also used for targeted and nontargeted experiments (see Figure 1). Concentrations and size distributions of the MCAs were obtained using a laser light obscuration and scattering device (Accusizer 780A, Particle Sizing Systems, Santa Barbara, CA).

Nontargeted lipid solutions were created using a 9:1 molar ratio of 1,2-distearoyl-sn-glycero-3-phosphocholine (DSPC-Powder, Avanti Polar Lipids, Alabaster, AL) and polyoxyethylene 40-stearate (PEG40S, Sigma, St. Louis, MO) in a 90 mL solution of phosphate-buffered saline (Fisher Scientific, Pittsburg, PA). Using a sonic dismembrator (Model 500, Fisher Scientific, Hampton, NH) for 15 seconds at 70% power in the presence of decafluorobutane (SynQuest Labs, Alachua, FL), MCAs were generated via acoustic emulsification and isolated with centrifugation processes optimized by Feshitan and colleagues.[22] Nontargeted unsorted distributions were created using the same batch of lipids and 1.5 mL was transferred to 3 mL vials. The vial was capped and decafluorobutane was exchanged with the air in the vial headspace using a custom vacuum apparatus. The vial was shaken vigorously for 45 seconds using a mixer (Vialmix, Bristol-Myers Squibb Medical Imaging, North Billerica, MA) to produce the characteristic polydisperse distribution for nontargeted in vivo experiments (see Figure 1).

MCAs designed to target $\alpha_v\beta_3$ integrins were created with a 9:0.5:0.5 molar ratio of DSPC-Powder, 1,2-distearoyl-snglycero-3-phosphoethanolmine-*N*-methoxy(polyethylene glycol)-2000 (DSPE-PEG2000, Avanti Polar Lipids), and DSPE-PEG2000 cross-linked to a cyclic RGD peptide (Cyclo-Arg-Ala-Asp-D-Tyr-Cys) (Peptides International, Louisville, KY) in a 90 mL solution of phosphate-buffered saline (Fisher Scientific, Pittsburgh). The same MCA size distributions were obtained as the perfusion studies using aforementioned centrifugation methods.

Animal Preparation and Contrast Administration

Sprague-Dawley rats were used for perfusion imaging, whereas molecular imaging was performed on both fibroscarcoma and R3230 mammary carcinoma tumor models in Fischer 344 rats. All animal studies were performed in accordance with protocols approved by the

University of North Carolina School of Medicine Institutional Animal Care and Use Committee.

During both targeted and perfusion ultrasound imaging studies, animals were anesthetized with 2 to 3% inhaled isoflurane anesthesia with oxygen and their body temperature was maintained through the use of a temperature-controlled heating pad. The area to be imaged was shaved, further depilated using a chemical hair remover, and then coupled to the ultrasound transducer using a water-based acoustic coupling gel.

A 24-gauge catheter was inserted into the tail vein of the animal for the administration of MCAs. In all experiments, bolus injections of 150 μL were delivered followed by an immediate flush of at least 100 μL sterile saline to clear any remaining MCAs from the catheter. Animals received less than a total of 1.5 mL of volume through the tail vein within a 24-hour period.

Perfusion Imaging

Both male and female albino Sprague-Dawley rats ($N = 9$) were used for nontargeted ultrasound perfusion imaging studies. Acoustic backscatter intensity data from the left kidney of each rat was obtained using a Siemens Sequoia Imaging System (Acuson Sequoia 512) in CPS mode with a 15 MHz linear array transducer (7 MHz in CPS mode) at a CPS gain of −5 dB. CPS was implemented to provide a high contrast to tissue ratio while being minimally destructive to MCAs.[2,30,34] For each study, the transducer was positioned in a fixed clamp to maintain the same imaging plane in each microbubble size experiment.

The aforementioned MCA size distributions were administered in the perfusion experiments (sorted 1 μm, sorted 3 μm, and unsorted polydisperse distributions). Each MCA size distribution was matched in terms of concentration and administered with bolus injections. MCA size distributions and concentrations were measured before and after administration by sampling the MCA storage container to ensure constancy over time for each subsequent animal injection. Injected dose concentrations ranged between 3×10^7 #/mL and 6×10^8 #/mL. The entire rat kidney was chosen as the region of interest (ROI) except in the cases where shadowing owing to acoustic attenuation occurred, specifically the sorted 3 μm distributions at high concentrations (150 μL at $\approx 6 \times 10^8$ #/mL). In these cases, only regions above the shaded area were included in the analysis; however, the same ROIs were compared for each individual distribution at the given concentration. Video data from perfusion experiments were acquired using the Siemens Sequoia imaging system and saved in compressed DICOM format. Perfusion imaging videos were imported and analyzed using custom *MATLAB* software (Mathworks, Natick, MA). Pixel intensity was averaged within the ROI for each video frame and normalized with respect to the movie frame with the highest mean. Within each data set, the system receive gain and transmit power were kept constant. The persistence time of the MCAs in the bloodstream was calculated by taking the time from the bolus injection to the time that the video intensity of the ROI reached half of the peak intensity, which is a method similar to that used previously.[11]

Tumor Models

Tumor models were established from propagated tumor tissue provided by Hong Yuan of the Dewhirst Lab at Duke University.[33] Prior to implantation, Fischer 344 rats were anesthetized using isoflurane and their left flank was shaved and disinfected. A 2 mm incision was made above the quad-riceps muscle and a ≈ 1 mm^3 piece of tumor tissue was subcutaneously placed. The incision was closed with a single suture. Imaging was performed on tumors after they had grown larger than 5 mm in the long axis.

Targeted Imaging

The relationship between MCA size and targeted agent sensitivity was assessed in three different rats and 22 different imaging planes. The transducer was mechanically adjusted across the tumor with a stage micrometer in 1 mm steps to acquire independent image planes with the use of fewer animals (independent planes were ensured as the −6 dB elevational beamwidth of the 15L8 in CPS mode is approximately 0.8 mm). Using control and $\alpha_v\beta_3$-targeted MCA populations at a dose concentration of 9×10^8 #/mL (150 μL bolus), the contrast sensitivity of unsorted and sorted 3 μm distributions was evaluated in each imaging plane. This could be determined only after freely flowing contrast agents had been completely removed from the system. The time required for the MCAs to clear was qualitatively determined to be on the order of 8 minutes for small size distributions and ≈ 30 minutes for large distributions. After sufficient time had passed, approximately 5 seconds of video data was collected in CPS mode with a gain of −3 dB, both to ensure that no freely flowing contrast agents were present and to determine the signal intensity of the bound contrast agents. In a study prior to the experiments presented here, the video intensity of targeted agents retained in vivo was observed over 30 seconds using CPS at a mechanical index of 0.18, and no loss in signal intensity was observed, indicating that our imaging parameters were nondestructive. The adherent bubbles were then destroyed using a high mechanical index (MI = 1.9) pulse sequence and then imaged again for 5 seconds with the initial CPS parameters to collect "background" image intensity. Within each data set, the system receive gain and transmit power were kept constant. Video data from targeting experiments were acquired using the Siemens Sequoia imaging system and saved in compressed DICOM format. The video files were exported and analyzed offline using *ImageJ* (public domain, National Institutes of Health, Bethesda, MD). Using B-mode image data collected prior to contrast administration, ROIs were determined around the perimeter of the tumor for each image plane. The difference between the predestruction pulse image and the background image was determined for each image plane as a measure of binding efficiency, similar to previous molecular imaging with ultrasound studies.[2,9] Analysis of targeted imaging results includes data from both fibrosarcoma and R3230 tumor models combined because imaging data collected from each tumor model showed similar video intensity enhancement with respect to MCA control populations.

Results

Perfusion Imaging (Intensity and Persistence)

Nontargeted perfusion imaging showed a strong correlation between backscatter intensity and the size and concentration of the MCAs administered. Example images at the peak intensities for three different diameter distributions at two different concentrations are presented (Figure 2). At low concentrations (150 μL at $\approx 3 \times 10^7$ #/mL), contrast circulation in the kidney from the sorted 1 μm and unsorted populations was barely visible at the tested gain setting (−5 dB), in contrast to the sorted 3 μm distribution. The normalized video intensity of sorted 3 μm MCAs was approximately 15 and 8 times larger than mean video intensities of the sorted 1 μm (0.77 ± 0.02 vs 0.05 ± 0.01; $p < .05$) and unsorted (0.77 ± 0.02 vs 0.09 ± 0.01; $p < .05$) populations, respectively.

At MCA concentrations greater than 2×10^8 #/mL (dose: 150 μL), mean video intensity produced by the various size distribution was not significantly different (sorted 3 μm: 0.94 ± 0.0005; sorted 1 μm: 0.80 ± 0.18; unsorted: 0.73 ± 0.30). In each case, the contrast agent circulation in the kidney could be readily visualized. This similarity in video intensity for different distributions at the higher concentration can likely be attributed to the video intensity saturation effect at the higher concentration. Hence, there was no apparent difference in contrast enhancement as a function of MCA distribution with a high enough

concentration and sufficient system receive gain. The ability of the sorted 3 μm MCA size distributions to clearly enhance the kidney microvasculature with approximately 20 times less dose than the sorted 1 μm and unsorted size distributions can be seen in Figure 3.

Persistence curves for the three different distributions (sorted 1 μm, sorted 3 μm, and unsorted) at two different concentrations (150 μL at 3×10^7 #/mL and 6×10^8 #/mL) are presented in Figure 4. These data show a direct relationship between MCA size and in vivo persistence. Microbubble circulation times increase significantly with size (Figure 5), which is expected given the relationship of bubble dissolution to MCA diameter.[20,27,28] The sorted 3 μm size distribution provides persistence times that are approximately 3 times (178 ± 9.9 seconds vs 52 ± 0.7 seconds: $p < .05$, concentration: 3×10^7 #/mL, dose: 150 μL) and approximately 9 times (455 ± 114 seconds vs 52 ± 7.8 seconds: $p < .05$, concentration: 6×10^8 #/mL, dose: 150 μL) greater than the persistence times of sorted 1 μm MCAs at the same concentrations. When comparing the sorted 3 μm distributions to unsorted polydisperse distributions, the persistence is approximately 3 times (178 ± 9.9 seconds vs 55 ± 16 seconds: $p < .05$, concentration: 3×10^7 #/mL, dose: 150 μL) and approximately 7 times (455 ± 114 seconds vs 65 ± 23 seconds: $p < .05$, concentration: 6×10^8 #/mL, dose: 150 μL) longer at low and high concentrations, respectively, which suggests a significant increase in circulation time for perfusion applications using larger MCAs.

Targeted Imaging

Targeted imaging studies showed a strong relationship between MCA size and targeted contrast sensitivity in both tumor models. Analysis of targeted imaging results includes data from both fibrosarcoma and R3230 tumor models combined because imaging data collected from each tumor model showed similar video intensity enhancement (Table 1) with respect to control populations.

Typical targeted CPS images overlaid onto the B-mode image of the rat tumor illustrate the relatively high acoustic contrast associated with sorted 3 μm MCAs compared to unsorted polydisperse distributions (Figure 6). At a CPS gain of −3 dB, video intensity provided from retention of targeted contrast agents in the tumor tissue was 17 times greater from the sorted 3 μm MCA distributions than from control (non-targeted) 3 μm populations (1.0 ± 0.35 vs 0.06 ± 0.06; $p < .05$) (Figure 7). The unsorted targeted MCAs also produced statistically significant contrast sensitivity improvement compared to unsorted control agents (0.05 ± 0.1 vs 0.01 ± 0.02; $p < .05$). Although the molecular imaging enhancement produced by both unsorted and sorted 3 μm targeted MCAs was statistically significant compared to that produced by nontargeted control agents, the contrast enhancement provided by the sorted 3 μm MCAs yielded a substantial improvement (20-fold greater) over the enhancement provided by the unsorted population (1.0 ± 0.35 vs 0.05 ± 0.1; $p < .05$).

Discussion

Previous studies have demonstrated that small quantities of MCAs may be retained at the target site.[6,7,9,10] Without optimal sensitivity to all adherent targeted contrast agents, sensitivity in ultrasonic molecular imaging is compromised. Prior in vitro studies have indicated that optimizing size of the microbubbles may result in increased contrast sensitivity.[6,19] Data presented here confirm that increased contrast sensitivity translates to the in vivo environment and that larger MCAs can increase signal in molecular imaging applications.

Our perfusion imaging studies demonstrated that at low concentrations (150 μL at 3×10^7 #/ mL) and a −5 dB gain on the imaging system, sorted 3 μm MCAs produced well-defined

enhancement of the kidney microvasculature. At the same low concentration, sorted 1 μm and unsorted MCAs offered no substantial contrast enhancement.

With the same system gain, and a concentration over a magnitude higher (6×10^8 #/mL, dose: 150 μL), the mean peak video intensity for all MCA distributions was similar and not statistically different, indicating that there was no advantage to the larger contrast agents at the higher concentration when a moderate (−5 dB) system receive gain is used. This was likely due to saturation of the video intensity for both MCA populations; hence, we cannot accurately evaluate results at the higher concentrations. It is likely that many researchers currently perform contrast imaging in this regime; hence, there may be little benefit of size-optimized bubbles if sufficient contrast concentration and system gain can be used. However, the focus of this study was to demonstrate the advantages of size optimization at low MCA concentrations, such as those present in ultrasonic molecular imaging.

Circulation persistence results indicated that sorted 3 μm MCAs produce at least 3 times greater circulation times than sorted 1 μm and unsorted MCA distributions at all tested concentrations, which is relevant in both clinical and targeted applications. These results are in agreement with data presented by Sirsi and colleagues, who illustrated that persistence time increased with microbubble size in a mouse model, as measured using high-frequency B-mode imaging.[20] In clinical practice, an increase in bloodstream persistence increases the time for diagnosis and maintains a longer time period during which the relative bubble concentration remains constant, which may be important for quantitative techniques. Perhaps the most important conclusion from these results, however, is that the time of image enhancement from larger microbubbles is not necessarily limited by increased filtration from the bloodstream, as one might hypothesize. Further studies will need to be performed to evaluate circulation time of microbubbles as a function of diameter range to establish what size range provides optimal enhancement while maintaining circulation time.

An increase in bloodstream persistence in targeted imaging provides a unique method to increase binding efficiency. Given that the probability of MCA adhesion is directly proportional to the number of passes through the circulatory system, and sorted 1 μm and unsorted size distributions have relatively short persistence times, sorted 3 μm MCA size distributions are more likely to bind to targeted tissue with their increased circulation times.[9,11,18,27,28] However, it is unclear from our targeted study what effect, if any, persistence has on the binding population between sorted 3 μm and sorted 1 μm MCA size distributions. The method for acoustically analyzing targeted agents used in this article relies on clearing the freely circulating bubbles from the circulatory system. Given that larger MCA distributions have longer bloodstream persistence times than smaller MCA size distributions, larger targeted MCAs have more time to bind to the targeted tissue. Therefore, the amount of signal intensity related to increased MCA size or increased binding efficiency is unknown. Ironically, this increased circulation time also complicates current targeted imaging techniques because of the need to wait for free agent clearance prior to imaging adherent bubbles. It should also be noted that there is most likely a tradeoff between wait time and binding efficiency. It is possible that the increase in cross-sectional area of the targeted agent is more susceptible to detachment owing to the increase in shear force by the circulatory system. However, we hypothesize that new techniques will allow near-real-time differentiation of free and adherent agents without waiting for clearance, which will alleviate this concern in the future.[14,15,35]

In this study, we used sorted 3 μm and unsorted MCA distributions to target angiogenic tumors to determine the relationship between contrast sensitivity enhancement and MCA size. Targeted imaging results showed a strong relationship between MCA size and targeted contrast sensitivity, with an observed 20-fold increase in video intensity provided by sorted

targeted 3 μm MCAs compared to unsorted targeted MCAs. Given the results of the presented perfusion studies and prior in vitro work, we assume that the increased backscatter intensity from the targeted sorted 3 μm bubbles was the main component in the sensitivity difference between large and small targeted populations.[22] However, larger microbubbles have a larger surface area, and it is reasonable to assume that they contain more binding ligands than small-diameter bubbles. Therefore, it is possible that the larger MCAs would have a higher probability of binding to a targeted site than smaller MCAs. In contrast, it is also likely that the larger microbubbles may detach faster than the smaller microbubbles owing to shear forces, as mentioned above. We are currently unable to assess these variables in vivo, but these aspects will be examined in future in vitro studies.

Data also showed that untargeted sorted 3 μm MCAs had a video intensity compared to baseline greater than that of the targeted unsorted agents. This discrepancy is probably due to a small population of nonspecifically bound MCAs in the circulatory system at the time of microbubble destruction. It is reasonable to assume that both sorted 3 μm and unsorted MCA control agents result in some nonspecific contrast adhesion; however, sorted 3 μm MCAs produce a larger backscatter intensity inadvertently creating higher values for control populations at a −3 dB gain setting. However, this small increase in signal from the 3 μm sorted control agents was minor compared to the large increase provided by the enhanced signal from the 3 μm targeted agents, so this did not detract notably from the achieved improvements in contrast sensitivity.

In this study, we have demonstrated that a several-fold improvement in contrast sensitivity enhancement can be achieved by tailoring MCA size distributions. This result is especially significant for ultrasonic molecular imaging applications, where the amount of targeted contrast agents retained is typically low, and maximum sensitivity to MCAs is desired. However, further work needs to be done on understanding persistence effects and binding probabilities related to increased microbubble diameter prior to further optimization of MCA size distributions for use in targeted ultrasound imaging. Additionally, further in vivo studies need to be performed to examine the optimization of the monodispersity of the bubble population and relationship of the mean diameter to the imaging frequency, which are not considered here.

Acknowledgments

References

1. Dayton PA, Ferrara KW. Targeted imaging using ultrasound. J Magn Reson Imaging. 2002; 16:362–77. [PubMed: 12353252]

2. Dayton PA, Rychak JJ. Molecular ultrasound imaging using microbubble contrast agents. Front Biosci. 2007; 12:5124–42. [PubMed: 17569635]

3. Liang HD, Blomley MJK. The role of ultrasound in molecular imaging. Br J Radiol. 2003; 76:S140–50. [PubMed: 15572336]

4. Lanza GM, Wickline SA. Targeted ultrasonic contrast agents for molecular imaging and therapy. Curr Probl Cardiol. 2003; 28:625–53. [PubMed: 14691443]

5. Villanueva FS, Lu EL, Bowry S, et al. Myocardial ischemia memory imaging with molecular echocardiography. Circulation. 2007; 115:345–52. [PubMed: 17210843]

6. Talu E, Hettiarachchi K, Zhao S, et al. Tailoring the size distribution of ultrasound contrast agents: possible method for improved sensitivity in molecular imaging. Mol Imaging. 2007; 6:384–92. [PubMed: 18053409]

7. Klibanov AL, Rychak JJ, Yang WC, et al. Targeted ultrasound contrast agent for molecular imaging of inflammation in high shear flow. Contrast Media Mol Imaging. 2006; 1:259–66. [PubMed: 17191766]

8. Ellegala DB, Leong-Poi H, Carpenter JE, et al. Imaging tumor angiogenesis with contrast ultrasound and microbubbles targeted to alphavbeta3. Circulation. 2003; 108:336–41. [PubMed: 12835208]

9. Lindner JR, Song J, Xu F, et al. Noninvasive ultrasound imaging of inflammation using microbubbles targeted to activated leukocytes. Circulation. 2000; 102:2745–50. [PubMed: 11094042]

10. Leong-Poi H, Christiansen J, Klibanov AL, et al. Noninvasive assessment of angiogenesis by ultrasound and microbubbles targetedto alpha(v)-integrins. Circulation. 2003; 107:455–60. [PubMed: 12551871]

11. Borden MA, Sarantos MR, Stieger SM, et al. Ultrasound radiation force modulates ligand availability on targeted contrast agents. Mol Imaging. 2006; 5:139–47. [PubMed: 16954028]

12. Zhao S, Borden M, Bloch SH, et al. Radiation-force assisted targeting facilitates ultrasonic molecular imaging. Mol Imaging. 2004; 3:135–48. [PubMed: 15530249]

13. Rychak JJ, Kilbanov AL, Ley KF, et al. Enhanced targeting of ultrasound contrast agents using acoustic radiation force. Ultrasound Med Biol. 2007; 33:1132–9. [PubMed: 17445966]

14. Zhao S, Kruse DE, Ferrara KW, et al. Acoustic response from adherent targeted contrast agents. J Acoust Soc Am. 2006; 120:EL63–9. [PubMed: 17225437]

15. Zhao S, Kruse DE, Ferrara KW, et al. Selective imaging of adherent targeted ultrasound contrast agents. Phys Med Biol. 2007; 52:2055–72. [PubMed: 17404455]

16. Rychak JJ, Lindner JR, Ley K, et al. Deformable gas-filled microbubbles targeted to P-selectin. J Control Release. 2006; 114:288–99. [PubMed: 16887229]

17. Weller G, Wong M, Modzelewski RA. Ultrasonic imaging of tumor angiogenesis using contrast microbubbles targeted via the tumor-binding peptide arginine-arginine-leucine. Cancer Res. 2005; 65:533–9. [PubMed: 15695396]

18. Quaia, E., editor. Contrast media in ultrasonography—basic principles and clinical applications. Springer; New York: 2005.

19. Kaya, M.; Feingold, S.; Streeter, J., et al. Acoustic characterization of individual monodisperse contrast agents with an optical-acoustical system.. Proceedings of the 2009 IEEE Ultrasonics Symposium.; 2009. p. 1813-1816.Digital Object Identifier: 10.1109/ULTSYM.2009.5441561

20. Sirsi, S.; Feshitan, J.; Homma, S., et al. High-frequency ultrasound imaging of sizeisolated microbubbles in mice.. Proceedings of the 2009 IEEE Ultrasonics Symposium.; 2009. p. 271-274.Digital Object Identifier: 10.1109/ULTSYM.2009.5441659

21. Hettiarachchi K, Talu E, Longo ML, et al. On-chip generation of microbubbles as a practical technology for manufacturing contrast agents for ultrasonic imaging. LabChip. 2007; 7:463–8.

22. Feshitan J, Chen C, Kwan J, et al. Microbubble size isolation by differential centrifugation. J Colloid Interface Sci. 2007; 329:316–24. [PubMed: 18950786]

23. Pancholi KP, Farook U, Moaleji R, et al. Novel methods for preparing phospholipid coated microbubbles. Eur Biophys J. 2007; 37:515–20. [PubMed: 17687548]

24. Farook U, Stride E, Edirisinghe M, et al. Microbubbling by co-axial electrohydrodynamic atomization. Med Biol Eng Comput. 2007; 45:781–9. [PubMed: 17624564]

25. Stride E, Edirisinghe M. Novel preparation techniques for controlling microbubble uniformity: a comparison. Med Biol Eng Comput. 2009 DOI: 10.1007/s11517-009-0490-8.

26. Farook U, Stride E, Edirisinghe M. Controlling size and size distribution of electrohydrodynamically prepared microbubbles. Bubble Sci Eng Technol. 2009; 1:53–7.

27. Borden MA, Longo ML. Dissolution behavior of lipid monolayer-coated, air-filled microbubbles: effect of lipid hydrophobic chain length. Langmuir. 2002; 18:9225–33.

28. Kabalnov A, Bradley J, Flaim S, et al. Dissolution of multi-component microbubbles in the bloodstream: 2. Experiment. Ultrasound Med Biol. 1998; 24:751–60. [PubMed: 9695278]

29. Sonne C, Xie F, Lof J, et al. Differences in Definity and Optison microbubble destruction rates at a similar mechanical index with different real-time perfusion systems. J Am Soc Echocardiogr. 2003; 16:1178–85. [PubMed: 14608290]

30. Stieger SM, Dayton PA, Borden MA, et al. Imaging of angiogenesis using cadence contrast pulse sequencing and targeted contrast agents. Contrast Media Mol Imaging. 2008; 3:9–18. [PubMed: 18335479]

31. Stieger SM, Bloch SH, Foreman O, et al. Ultrasound assessment of angiogenesis in a Matrigel model in rats. Ultrasound Med Biol. 2006; 32:673–81. [PubMed: 16677927]

32. Chomas JE, Pollard RE, Sadlowski AR, et al. Contrast-enhanced US of microcirculation of superficially implanted tumors in rats. Radiology. 2003; 229:439–46. [PubMed: 14526091]

33. Jung KH, Lee KH, Paik JY, et al. Favorable biokinetic and tumor-targeting properties of 99mTc-labeled glucosamino RGD and effect of paclitaxel therapy. J Nucl Med. 2006; 47:2000–7. [PubMed: 17138743]

34. Paul, D.; Phillips, PJ. Siemens Medical Whitepaper. Siemens; Mountain View (CA): 2005. Cadence contrast agent imaging technology on the ACUSON Sequoia Ultrasound Platform..

35. Needles A, Couture O, Foster FS. A method for differentiating targeted microbubbles in real time using subharmonic micro-ultrasound and interframe filtering. Ultrasound Med Biol. 2009; 35:1564–73. [PubMed: 19632763]
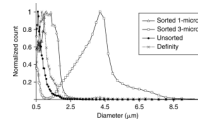
Figure 1.
Example microbubble contrast agent size distributions obtained during centrifugal size sorting. Values were normalized to the maximum count for comparison.
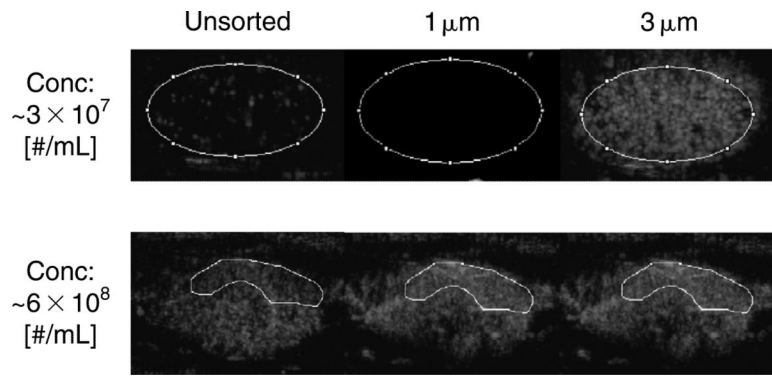
Figure 2.
Example cadence pulse sequencing images of nontargeted kidney perfusion data for sorted and unsorted microbubble distributions. Regions of interest are indicated and constant for each concentration set. All images were taken at the peak mean intensity.
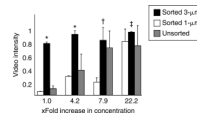
Figure 3.
Mean normalized peak video intensity as a function of concentration for nontargeted size-sorted perfusion studies. Mean peak values of intensity per region of intensity were normalized across concentration data sets to the maximum average peak intensity. Concentration values are a factor of baseline concentration (150 μL at 3×10^7 #/mL). *$p < .05$ compared to sorted 1 μm and unsorted microbubble contrast agents (MCAs).†$p < .05$ compared to sorted 1 μm and $p < .07$ compared to unsorted MCAs. ‡$p < .25$ compared to sorted 1 μm and unsorted MCAs.
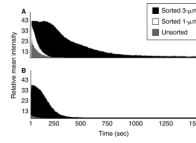
Figure 4.
Example persistence curves for nontargeted size-sorted and unsorted microbubble distributions. *A*, Example persistence curves at a concentration of 3×10^7 #/mL (dose: 150 μL). *B*, Example persistence curves at a concentration of 6×10^8 #/mL (dose: 150 μL).
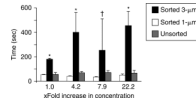
Figure 5.
Mean persistence times as a function of concentration for nontargeted size-sorted and unsorted perfusion studies. Persistence times were taken to be time from the bolus injection to the time that the video intensity of the region of interest reached half of the peak intensity. * $p < .05$ compared to sorted 1 μm and unsorted microbubble contrast agents (MCAs). $^{†}p = .$ 1 compared to sorted 1 μ and unsorted MCAs.
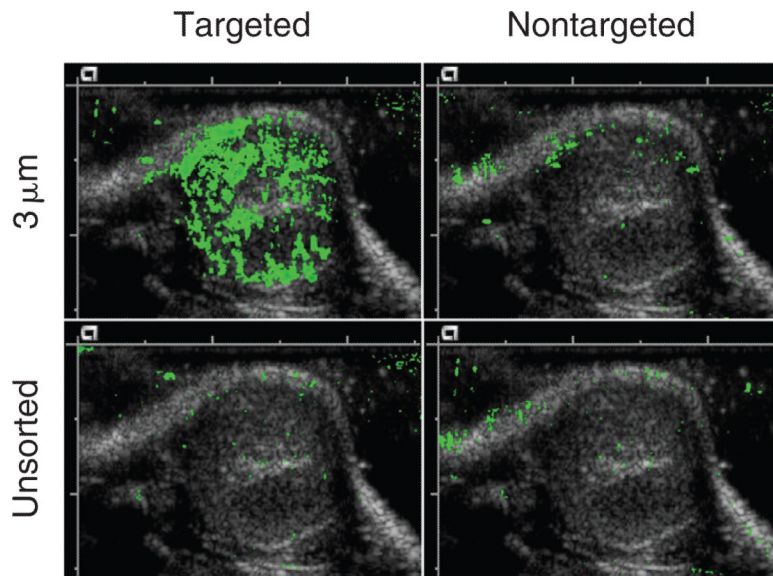
Figure 6.
Example of image-subtracted targeted and nontargeted data for sorted and unsorted microbubble distributions overlaid with their respective B-mode images.
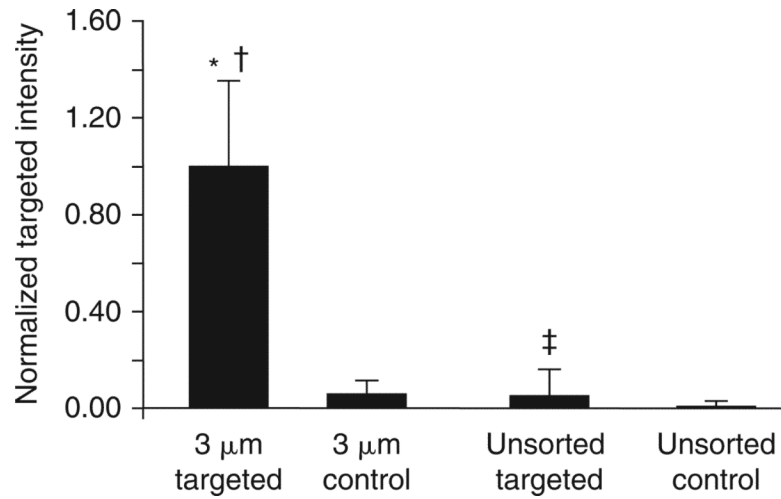
Figure 7.
Normalized mean video intensity for targeted and non-targeted large and unsorted microbubble distributions. Mean video intensity was taken to be the difference between the mean targeted region of interest (ROI) image section and the mean baseline ROI image section. $*p < .05$ compared to unsorted targeted microbubble contrast agents (MCAs). $^{\dagger}p < .05$ compared to 3 μm control MCAs. $^{\ddagger}p < .05$ compared to unsorted control MCAs.

Table 1

Normalized Mean Targeted Video Intensity Comparison between Fibrosarcoma and R3230 Tumor Models for Sorted 3 μm and Unsorted Populations (Targeted and Nontargeted)

	Normalized Mean Targeted Video Intensity	
	Fibrosarcoma Tumor Model	R3230 Tumor Model
Sorted 3 μm targeted	0.95 ± 0.31	1.11 ± 0.08
Sorted 3 μm nontargeted	0.03 ± 0.03	0.11 ± 0.08
Unsorted targeted	0.07 ± 0.13	0.01 ± 0.02
Unsorted nontargeted	0.01 ± 0.02	0.00 ± 0.01